

Cite this article as: Zhang Han, Sang Chen, Zhang Yan, et al. Hot Deformation Behavior and Microstructure Evolution of Electrolytic Copper[J]. Rare Metal Materials and Engineering, 2025, 54(04): 920-929. DOI: <https://doi.org/10.12442/j.issn.1002-185X.20240168>.

ARTICLE

Hot Deformation Behavior and Microstructure Evolution of Electrolytic Copper

Zhang Han^{1,2}, Sang Chen^{1,2}, Zhang Yan³, Xu Yangtao^{1,2}, Qiao Jisen^{1,2}, Xia Tiandong^{1,2}

¹School of Materials Science and Engineering, Lanzhou University of Technology, Lanzhou 730050, China; ²State Key Laboratory of Advanced Processing and Recycling of Nonferrous Metals, Lanzhou University of Technology, Lanzhou 730050, China; ³Jinchuan Group Copper Co., Ltd, Jinchang 737100, China

Abstract: The hot deformation behavior of electrolytic copper was investigated using a Gleeble-3500 thermal simulation testing machine at temperatures ranging from 500 °C to 800 °C and strain rates ranging from 0.01 s⁻¹ to 10 s⁻¹, under 70% deformation conditions. The true stress-true strain curves were analyzed and a constitutive equation was established at a strain of 0.5. Based on the dynamic material model proposed by Prasad, processing maps were developed under different strain conditions. Microstructure of compressed sample was observed by electron backscatter diffraction. The results reveal that the electrolytic copper demonstrates high sensitivity to deformation temperature and strain rate during high-temperature plastic deformation. The flow stress decreases gradually with raising the temperature and reducing the strain rate. According to the established processing map, the optimal processing conditions are determined as follows: deformation temperatures of 600–650 °C and strain rates of 5–10 s⁻¹. Discontinuous dynamic recrystallization of electrolytic copper occurs during high-temperature plastic deformation, and the grains are significantly refined at low temperature and high strain rate conditions.

Key words: electrolytic copper; hot deformation; constitutive equation; dynamic recrystallization

1 Introduction

Copper is widely used in various industries, including aerospace, electronics, energy, magnetic materials, etc, due to its outstanding properties such as corrosion resistance, ductility, electrical conductivity and strength^[1-6]. In recent years, with the full coverage of 4G mobile communications, 5G communications engineering construction, and the rapid development of new energy vehicles, new consumer terminals rapidly emerge, which will increase the demand for copper processed materials. Traditionally, the pre-processing for rolled copper industry involves several steps: extracting copper from ores, smelting, electrolytic purification, casting into ingots, acid washing, degreasing, repeated hot rolling, and finally processing into foils. However, the future development of copper strips is focused on enhancing key attributes such as strength, conductivity, precision, quality, and stability.

Concurrently, there is a strong emphasis on adopting more refined and energy-efficient production processes with shorter cycles. This shift toward energy conservation and environmentally friendly practices necessitates inevitable transformations and upgrades within the copper strip industry.

To establish optimal thermal processing methods, extensive research has been conducted on the thermal deformation behavior and microstructural evolution of pure copper and copper alloys. These studies have established constitutive equations that can predict true stress-true strain changes under different deformation conditions^[7]. By considering strain hardening and dynamic and static softening mechanisms, the resulting flow stress models demonstrate applicability even under substantial plastic deformation^[8]. Notably, during high-temperature plastic deformation, the influence of temperature and strain rate on the flow stress of copper and its alloys is significant, i. e., stress decreases gradually with raising

Received date: April 22, 2024

Foundation item: Gansu Province Higher Education Institutions Industrial Support Program Project (2022CYZC-19); Gansu Provincial Science and Technology Major Project (22ZD6GA008)

Corresponding author: Xia Tiandong, Ph. D., Professor, State Key Laboratory of Advanced Processing and Recycling of Nonferrous Metals, Lanzhou University of Technology, Lanzhou 730050, P. R. China, Tel: 0086-931-2976933, E-mail: xiatid@lut.edu.cn

Copyright © 2025, Northwest Institute for Nonferrous Metal Research. Published by Science Press. All rights reserved.

temperatures or reducing strain rates^[9-10]. At higher strain rates ($10^3 - 10^4 \text{ s}^{-1}$), twinning has a minimal effect on the deformation of pure copper under quasistatic conditions. However, its nucleation rate notably increases at high strain rates^[11]. Through the use of material dynamic models combined with microscopic observations, researchers have identified a high power dissipation coefficient in pure copper, which corresponds to the stable region of dynamic recrystallization, with an unstable region observed within the strain rate range of $0.01 - 0.1 \text{ s}^{-1}$ ^[7,12]. Additionally, research on the misorientation distribution between deformation-induced and original grain boundaries in copper shows an evolution from low-angle to high-angle boundaries with increasing the strain^[13]. Notably, Prasad et al^[14] studied the thermal deformation behavior of electrolytic copper across temperatures from $300 \text{ }^\circ\text{C}$ to $950 \text{ }^\circ\text{C}$ and strain rates from 0.001 s^{-1} to 1 s^{-1} . They found that at $400 - 600 \text{ }^\circ\text{C}$, the activation energy was 159 kJ/mol , and it increased to 198 kJ/mol at $700 - 950 \text{ }^\circ\text{C}$.

Although there are relatively few reports on the direct thermal deformation of electrolytic copper, understanding its behavior and microstructural evolution during plastic deformation is pivotal for developing an efficient process for the direct rolling of electrolytic copper plates. This study investigated the thermal deformation behavior of electrolytic copper across various deformation temperatures and strain rates using the Gleeble-3500 thermal simulation machine, aiming to elucidate the microstructural evolution during this process.

2 Experiment

The electrolytic copper used for the experimental material was the cathode copper plate prepared by a company with the traditional method. The process involved the utilization of crude copper as the anode and pure copper as the cathode, which were immersed in an electrolyte solution primarily

consisting of copper sulfate. During electrification, pure copper was precipitated on the cathode plates. The detailed chemical composition is shown in Table 1. Fig. 1 shows that the deposition layer of electrolytic copper and the copper initiator sheet are clearly separated by an interface. The white dotted line box area is the interface between the copper starting sheet and the deposition layer. Region 1 and region 2 are microstructures of the deposition layer and the copper starting sheet, respectively. At the interface between the deposition layer and the copper starting sheet, grains predominantly exhibit columnar structures with uneven distribution and numerous twins. In addition, the grains at this interface exhibit a finer morphology compared to those located farther away, with a scale of approximately $5 \mu\text{m}$.

Cylindrical samples measuring $\Phi 8 \text{ mm} \times 12 \text{ mm}$ were prepared by wire cutting. These samples underwent surface polishing before single-pass isothermal compression experiments on a Gleeble-3500 thermal simulation machine. The experiments were conducted at different deformation temperatures and strain rates. All samples were heated to $800 \text{ }^\circ\text{C}$ at a heating rate of $10 \text{ }^\circ\text{C/s}$, held for 3 min, then cooled at the same rate to the deformation temperature, held for another 3 min, and subjected to compression experiments. Immediate water cooling post-compression was implemented to preserve the high-temperature deformation microstructure of the electrolytic copper, as depicted in Fig. 2. The compression was set at 70%, at deformation temperatures of $500, 600, 700,$ and $800 \text{ }^\circ\text{C}$ and strain rates of $0.01, 0.1, 1,$ and 10 s^{-1} . During the compression process, tantalum and graphite pieces were inserted to reduce friction. Additionally, high-temperature lubricants were applied.

The post-deformation samples were radially cut for observing microstructural changes. The samples were electrochemically polished at room temperature in a solution consisting of 5% hydrochloric acid and 95% alcohol at 30 V for approximately 25–30 s. The microstructure analysis was conducted using an Oxford-SYMMERY electron backscatter

Table 1 Main impurity element content of electrolytic copper (wt%)

Se	Te	Bi	Sb	As	Pb	S	Fe	Ag	Total
0.0002	0.0002	0.0002	0.0004	0.0005	0.0005	0.0015	0.001	0.0025	0.007

diffraction (EBSD) at an electron-accelerating voltage of 15 kV. The EBSD data were processed using Channel 5 software.

3 Results and Discussion

3.1 True stress-true strain curves during thermal deformation of electrolytic copper

Fig. 3 shows the true stress-true strain behavior of electrolytic copper with 70% deformation at different strain rates and deformation temperatures. Fig. 3a and 3b illustrate a consistent trend: after the peak stress, the flow stress gradually decreases as the strain increases. This phenomenon is primarily due to the interplay between work hardening, dynamic recovery, and dynamic recrystallization mechanisms

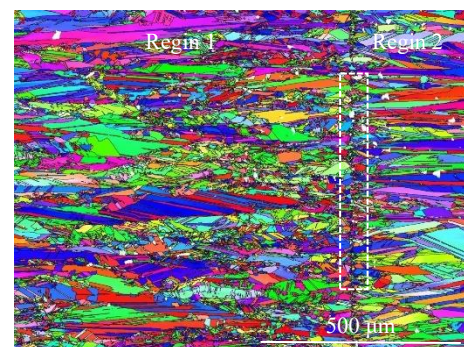


Fig. 1 Microstructure of untreated electrolytic copper

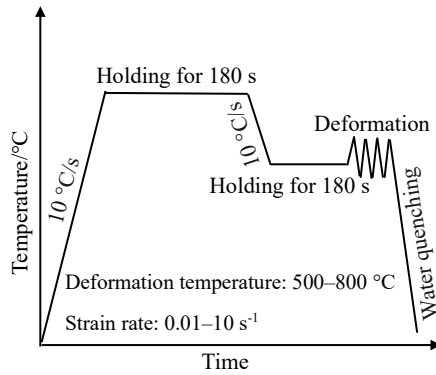


Fig.2 Schematic diagram of compression process of electrolytic copper

during the thermal deformation process^[15–16].

During the initial stage of thermal deformation, the rheological stress increases rapidly with very small strain changes, and reaches its peak at a certain strain value. This phenomenon is due to the gradual increase in dislocation density within the material as plastic deformation advances, which is a process dominated by work hardening. At a certain strain rate (0.01, 0.1, 1, and 10 s⁻¹), the rheological stress of electrolytic copper decreases with increasing the deformation temperature, and all the peak stress points tend to shift to the left.

Following the peak stress, the flow stress exhibits a gradual decline with increasing strain until reaching a steady-state level. Notably, there is a slight increase in peak stress as strain continues to increase. In this stage, the softening effect

induced by dynamic recrystallization counteracts work hardening, leading to the declining trend in flow stress with increasing strain in electrolytic copper.

Moreover, Fig.3 underscores the influence of deformation temperature on flow stress under constant strain rates, depicting a gradual decrease as deformation temperature rises. This is because thermal activation capability of electrolytic copper is enhanced at high temperatures, resulting in a decrease in dislocation density and weakening work hardening effects.

3.2 Establishing the constitutive equation of electrolytic copper

In high-temperature plastic deformation, it is crucial to understand the relationship between flow stress and deformation parameters such as temperature and strain rate, and strain is crucial. The Arrhenius equation was proposed by Sellars et al^[17], which can describe the response law between the rheological stress of the material and each parameter^[18–19]. This equation presents three different forms: exponential at low-stress levels ($\alpha\sigma < 0.8$), power-law at high-stress levels ($\alpha\sigma > 1.2$), and hyperbolic-sine at arbitrary stress levels, as shown in Eq. (1)–Eq. (3), respectively. Jenab et al^[20] found that the hyperbolic-sine form is a better characterization of flow stress changes in high-temperature plastic deformation.

$$\dot{\epsilon} = A_1 \sigma^{n_1} \exp\left(-\frac{Q}{RT}\right) \quad (1)$$

$$\dot{\epsilon} = A_2 \exp(\beta\sigma) \exp\left(-\frac{Q}{RT}\right) \quad (2)$$

$$\dot{\epsilon} = A [\sinh(\alpha\sigma)]^n \exp\left(-\frac{Q}{RT}\right) \quad (3)$$

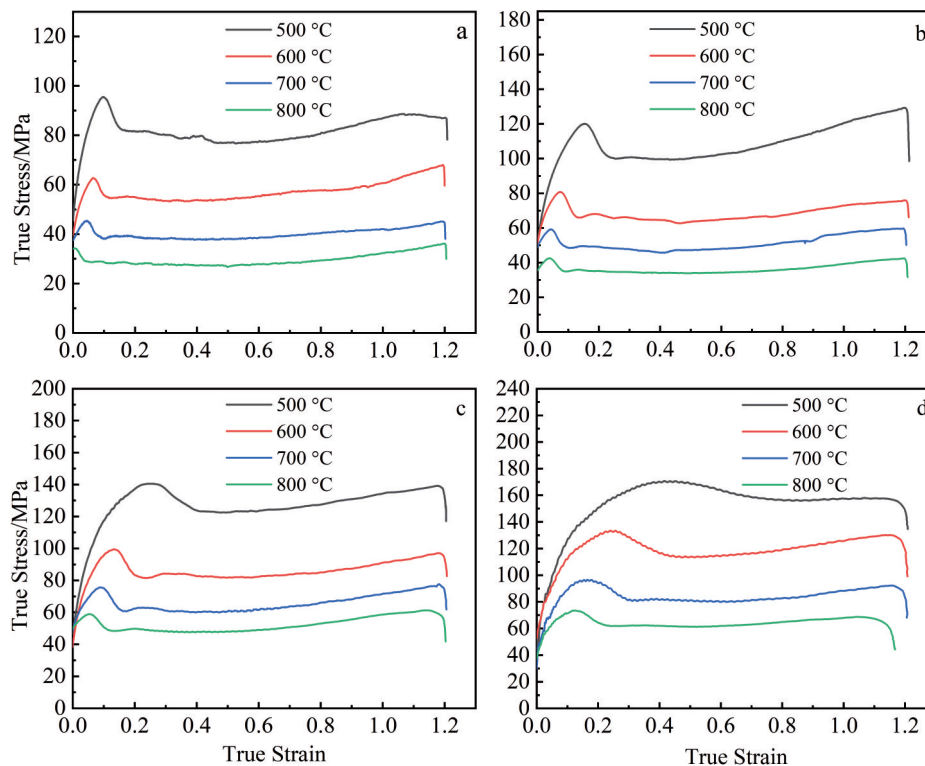


Fig.3 True stress-true strain curves of electrolytic copper at different strain rates: (a) 0.01 s⁻¹, (b) 0.1 s⁻¹, (c) 1 s⁻¹, and (d) 10 s⁻¹

where $A, A_1, A_2, n_1, \alpha,$ and β are material-dependent constants, and $\alpha=\beta/n_1$; $\dot{\epsilon}$ is the strain rate (s^{-1}); n is the stress exponent; Q is the deformation activation energy (kJ/mol); R is the gas constant; T is the absolute temperature (K).

Taking logarithms on both sides of Eq.(1-3) simultaneously, Eq.(4-6) can be obtained, respectively:

$$\ln \dot{\epsilon} = n_1 \ln \sigma + \ln A_1 - \frac{Q}{RT} \quad (4)$$

$$\ln \dot{\epsilon} = \beta \sigma + \ln A_2 - \frac{Q}{RT} \quad (5)$$

$$\ln \dot{\epsilon} = n \ln [\sinh(\alpha\sigma)] + \ln A - \frac{Q}{RT} \quad (6)$$

These equations enable the determination of constants like stress exponent (n_1), β , and α . Linear fitting of the data in Fig. 4 at each temperature yields the following values at a strain of 0.5: $n_1=8.806$ 81, $\beta=0.133$ 24, and $\alpha = \beta/n_1 = 0.015$ 12.

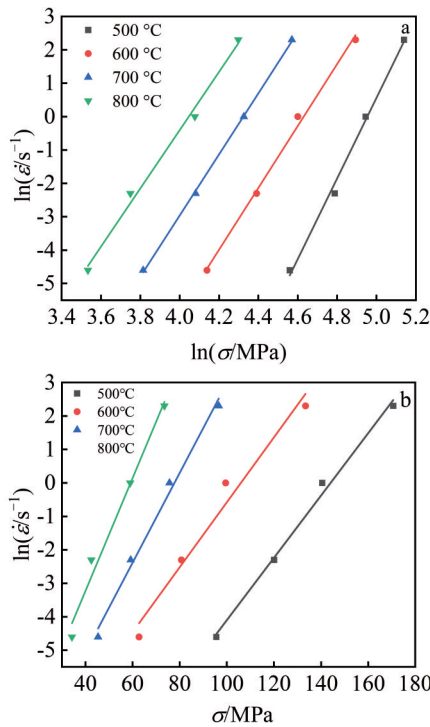


Fig.4 Linear relationships of $\ln \dot{\epsilon}$ vs. $\ln \sigma$ (a) and $\ln \dot{\epsilon}$ vs. σ (b)

In Eq. (6), the flow stress depends on both deformation temperature and strain rate. Eq. (7) can be derived by taking partial derivatives under constant deformation temperature or strain rate conditions. This equation enables the determination of the deformation activation energy Q for electrolytic copper.

At a constant deformation temperature, a plot of $\ln \dot{\epsilon}$ vs. $\ln[\sinh(\alpha\sigma)]$ is depicted in Fig. 5a. The correlation coefficient of 0.956 65, obtained from linear regression analysis, indicates a significant linear relationship between $\ln \dot{\epsilon}$ and $\ln[\sinh(\alpha\sigma)]$. The average slope of the four fitted lines, denoted as $m=3.998$ 38, is obtained.

Similarly, at a constant strain rate, a plot of $\ln[\sinh(\alpha\sigma)]$ against $1000/T$ is shown in Fig. 5b. The linear regression analysis shows a linear relationship between $\ln[\sinh(\alpha\sigma)]$ and $1000/T$, with a correlation coefficient above 0.985 31. The average slope of the four fitted lines, denoted as $n = 6.296$ 92, gives the determination of $Q=209.32$ kJ/mol.

Electrolytic copper is a highly pure form of copper. Ref. [9, 13, 21] summarized that in pure copper, the activation energy is affected by the deformation temperature, strain rate, and composition. This suggests that the activation energy is more sensitive to the deformation parameter, resulting in different Q . The activation energy range is 159–245 kJ/mol. The experimentally calculated activation energy falls within this range, confirming its reasonability.

$$Q = R \left. \frac{\partial \ln[\sinh(\alpha\sigma)]}{\partial \ln \dot{\epsilon}} \right|_{\dot{\epsilon}} \left. \frac{\partial \ln \dot{\epsilon}}{\partial \ln[\sinh(\alpha\sigma)]} \right|_T \quad (7)$$

Zener et al^[22] considered a functional relationship between strain rate and deformation temperature during high-temperature plastic deformation, and introduced a temperature-compensated strain rate factor, Z , in the Zener-Hollomon parameters, as shown in the comprehensive expression in Eq. (8). Eq. (9) is obtained by taking the logarithm on both sides of Eq.(8). Utilizing the calculated deformation activation energy, Q , to obtain $\ln Z$, a linear fit between $\ln Z$ and $\ln[\sinh(\alpha\sigma)]$ is depicted in Fig.6. The intercept of this fitting line corresponds to $\ln A=25.119$ 42, and thus $A=8.11 \times 10^{10}$.

Through the above calculations, the relevant parameters of the constitutive equation at a strain of 0.5 are obtained, as shown in Table 2.

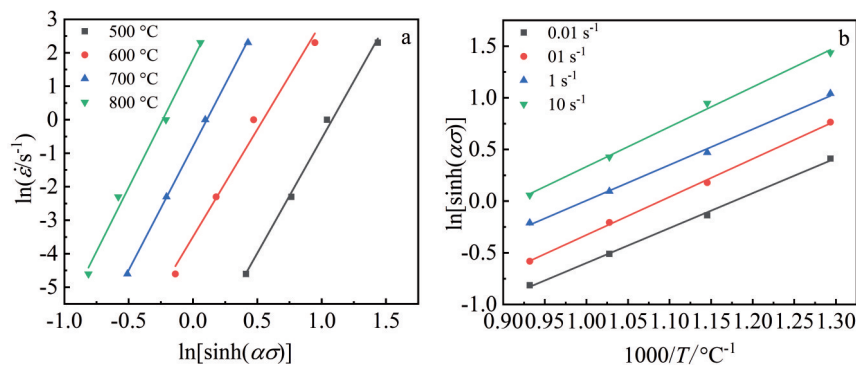


Fig.5 Fitting of $\ln \dot{\epsilon} - \ln[\sinh(\alpha\sigma)]$ (a) and $\ln[\sinh(\alpha\sigma)] - 1000/T$ (b) at different deformation temperatures

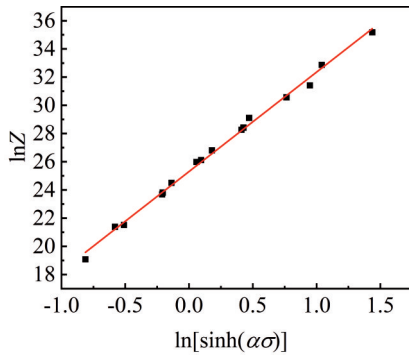


Fig.6 Relation between $\ln Z$ and $\ln[\sinh(\alpha\sigma)]$

$$Z = \dot{\epsilon} \exp\left(\frac{Q}{RT}\right) = A[\sinh(\alpha\sigma)]^n \quad (8)$$

$$\ln Z = \ln \dot{\epsilon} + \frac{Q}{RT} = \ln A + n \ln[\sinh(\alpha\sigma)] \quad (9)$$

Substituting the calculated values of the parameters (α , Q , n , and A) into Eq.(3), the constitutive equation for electrolytic copper during thermal deformation can be established at a strain of 0.5:

$$\dot{\epsilon} = 8.11 \times 10^{10} [\sinh(0.01512\sigma)]^{6.29692} \exp\left(\frac{-209.32}{RT}\right) \quad (10)$$

3.3 Building and analysis of thermal processing maps

The dynamic materials model (DMM) provides a thermal processing map that is crucial for assessing workability^[23]. This map visually represents a material's plastic deformation capability under various deformation temperatures and strain rates, serving as a valuable tool for predicting workability and microstructure evolution during deformation. It provides a certain reference for the determination of a reasonable thermal processing methods^[24-25].

According to DMM theory, the energy consumption during deformation consists of two components: energy required for plastic deformation (G) and the energy consumed during structure evolution (J). The ratio between these energies is determined by the strain rate sensitivity index (m) under specific stress conditions:

$$m = \frac{\partial J}{\partial G} = \frac{\partial \lg \sigma}{\partial \lg \dot{\epsilon}} \quad (11)$$

The power dissipation coefficient, $\eta = 2m/(m+1)$, reflects variations in deformation temperature and strain rate when strain is constant. Eq. (12) presents Prasad's instability criterion, which uses the ζ value to predict the flow instability region of electrolytic copper.

$$\zeta(\dot{\epsilon}) = \frac{\partial \ln\left(\frac{m}{m+1}\right)}{\partial \ln \dot{\epsilon}} + m < 0 \quad (12)$$

The thermal processing map for electrolytic copper can be generated by overlaying the power dissipation map and the

flow instability map. Fig.7 illustrates this map at strains of 0.3, 0.4, and 0.5. The gray area indicates instability region, while white denotes safety region. At a strain of 0.3, instability primarily occurs at low temperatures+high strain rates, high temperatures+high strain rates, and moderate temperatures+low strain rates. At a strain of 0.5, instability decreases at low temperatures and high strain rates, while it becomes more concentrated at low temperatures and low strain rates, as well as high temperatures and high strain rates. A higher power dissipation factor indicates a greater probability of dynamic recrystallization, which is considered as a safe processing zone. Between strains of 0.3 and 0.5, regions with a power dissipation factor exceeding 0.22 are identified as the optimal processing parameters for electrolytic copper. The optimal deformation temperatures range from 600 °C to 650 °C, and the optimal strain rates range from 5 s⁻¹ to 10 s⁻¹.

In order to further clarify the microstructure changes corresponding to the instability region and the safety region, an example of thermal processing diagram with a true strain of 0.5 is analyzed, as shown in Fig.7c.

In Fig. 7c, region I shows the microstructure machined in the safe region (deformation temperature of 500 °C and strain rate of 0.01 s⁻¹). It can be observed that electrolytic copper undergoes dynamic recrystallization under specified deformation conditions in this region, and the grain size is basically uniformly. Due to the homogeneous microstructure, copper cathodes have higher plastic processability under these deformation conditions. Region II shows the microstructure machined in the destabilized region (deformation temperature of 500 °C and strain rate of 10 s⁻¹). It can be observed that electrolytic copper undergoes partial dynamic recrystallization under these deformation conditions. Some small recrystallized grains are present in the form of "necklaces", and the grain size distribution is very uneven. This deformation range may be the cause of the destabilization of electrolytic copper. Region III shows the microstructure machined in the destabilized region (deformation temperature of 800 °C and strain rate of 10 s⁻¹). It can be observed that the grains of electrolytic copper are significantly coarsened, due to adiabatic temperature rise in a short period of time at high temperatures and high strain rates, resulting in abnormal grain growth. Thus, electrolytic copper is not suitable for plastic deformation in this region.

3.4 Effect of deformation temperature and strain rate on microstructure

3.4.1 IPF analysis

To study how deformation temperature and strain rate influence the microstructure of electrolytic copper during deformation, EBSD analyses were performed on samples under varying parameters. Fig. 8a – 8c display inverse pole

Table 2 Parameters related to the constitutive equation at true strain of 0.5

α	β	n	m	$Q/\text{kJ}\cdot\text{mol}^{-1}$	$\ln A$	A
0.015 12	0.133 24	6.296 92	3.998 38	209.32	25.119 42	8.11×10^{10}

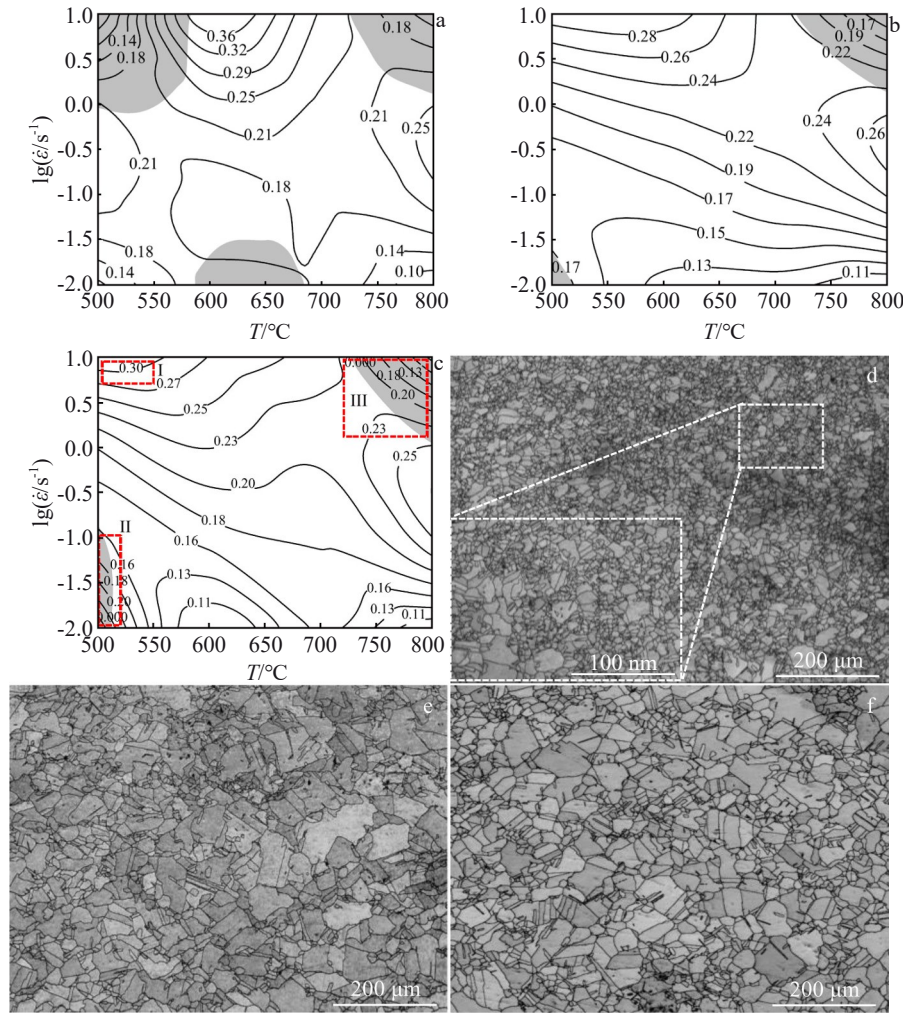


Fig.7 Thermal processing maps of electrolytic copper at strains of 0.3 (a), 0.4 (b), and 0.5 (c); microstructures machined under parameters of regions I (d), region II (e), and region III (f) marked in Fig.7c

figures (IPFs) at a deformation temperature of 500 °C and strain rates of 0.01, 0.1 and 1 s⁻¹, respectively. Meanwhile, Fig. 8d – 8g exhibit IPFs at a strain rate of 10 s⁻¹ and deformation temperatures of 500, 600, 700, and 800 °C, respectively. Different colors in the images represent distinct crystal orientation relationships.

At 500 °C and low strain rate (0.01 s⁻¹), there are a few “necklace-like structures” and minor dynamically recrystallized grains at original grain boundaries, signifying the early stage of dynamic recrystallization under these conditions. As the strain rate increases from 0.01 s⁻¹ to 10 s⁻¹, finer recrystallized grains progressively nucleate at triple junctions and serrated grain boundaries, as highlighted in the rectangular box in Fig. 8b. Additionally, the grain size decreases noticeably as strain rate rises. Although dislocations accumulation occurs, they are eventually annihilated. However, at high strain rates (10 s⁻¹), due to the extremely short deformation time, dislocation accumulation overtakes annihilation. Moreover, grain growth, which is thermally activated and time-dependent, becomes significantly constrained at high strain rates, leading to noticeable grain

refinement (Fig. 8c). At low temperatures and high strain rates, significant dynamically recrystallized grains near grain boundaries are observed, showcasing “grain boundary bulging” and “necklace-like structure” (Fig. 8d). These morphological characteristics confirm the predominance of discontinuous dynamic recrystallization during the thermal plastic deformation of electrolytic copper. Moreover, a substantial distribution of recrystallized grains in “necklace-like” form within the matrix further indicates the prevalence of dynamic recrystallization under these conditions. When the deformation temperature is 600 °C (Fig. 8e), considerable grain growth occurs. The temperature exerts a more pronounced effect on atomic diffusion and grain boundary migration, inducing significant grain growth with a relatively heterogeneous microstructure.

3.4.2 Analysis of grain boundaries and their orientation differences

Fig. 9 illustrates grain boundary and grain boundary orientation maps of electrolytic copper across varying deformation temperatures (600 and 800 °C) and strain rates (0.01 and 10 s⁻¹). Different colors denote distinct grain boundaries:

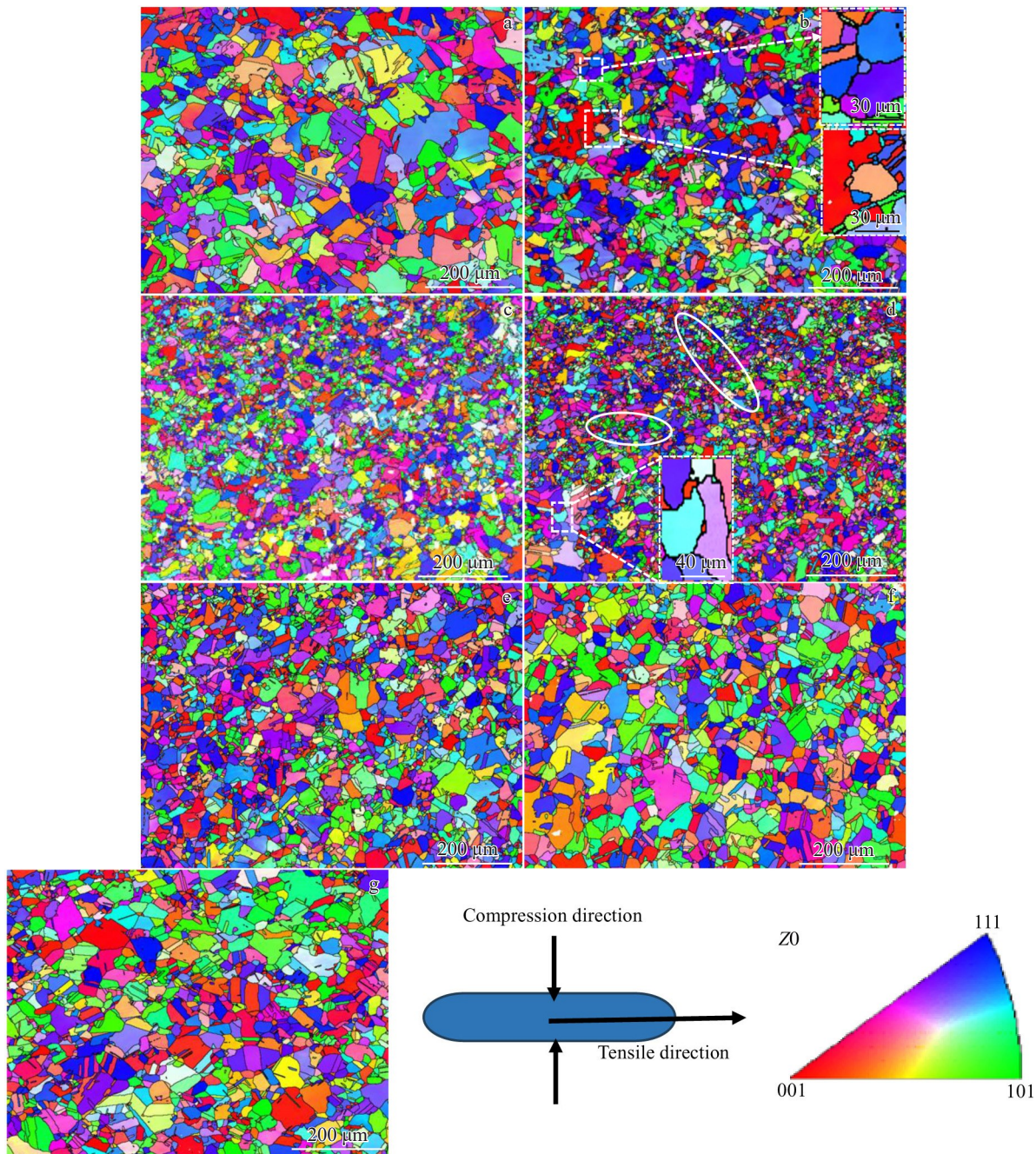


Fig.8 IPFs of electrolytic copper under different deformation conditions: (a) 500 °C, 0.01 s⁻¹; (b) 500 °C, 0.1 s⁻¹; (c) 500 °C, 1 s⁻¹; (d) 500 °C, 10 s⁻¹; (e) 600 °C, 10 s⁻¹; (f) 700 °C, 10 s⁻¹; (g) 800 °C, 10 s⁻¹

green for low-angle grain boundaries (LAGBs, $2^\circ \leq \theta \leq 15^\circ$), black for high-angle grain boundaries (HAGBs, $\theta > 15^\circ$), and red for twin boundaries ($\langle 111 \rangle 60^\circ$).

At strain rate of 10 s⁻¹ and deformation temperatures of 600 and 800 °C (Fig.9a–9b), LAGBs account for 3.4% and 2.2%, respectively, indicating that during dynamic recrystallization of electrolytic copper, the transition from LAGBs to HAGBs progressively increases as deformation temperature rises. Moreover, the dynamically recrystallized grains noticeably grow with increasing the temperature. Concurrently, at a strain rate of 10 s⁻¹, the proportion of twin boundaries increases at higher deformation temperature.

At deformation temperature of 500 °C (Fig.9c–9d), during dynamic recrystallization under both low (0.01 s⁻¹) and high (10 s⁻¹) strain rates, the proportion of LAGB gradually increases to 3.3% and 3.6%, respectively, with elevating strain rate. In contrast, the percentages of HAGB and twin boundaries increase. Additionally, the grain boundary orientation distribution maps reveal a bimodal orientation distribution of grain boundaries in electrolytic copper during dynamic recrystallization at different deformation temperatures and strain rates. The distribution of grain boundary is significantly influenced by both deformation temperature and strain rate.

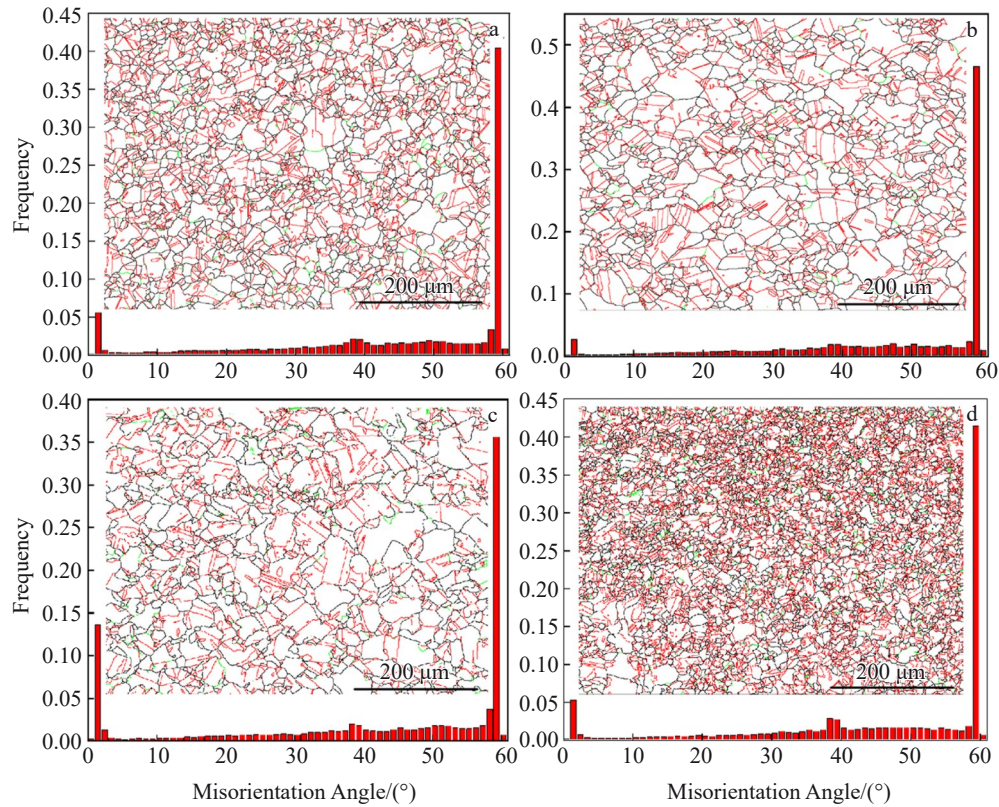


Fig.9 Grain boundary maps and orientation distributions of electrolytic copper under different deformation conditions: (a) 600 °C, 10 s⁻¹; (b) 800 °C, 10 s⁻¹; (c) 500 °C, 0.01 s⁻¹; (d) 500 °C, 10 s⁻¹

3.4.3 Dynamic recrystallization analysis

Fig. 10 shows the distribution of dynamic recrystallization grains in electrolytic copper at different deformation

temperatures and strain rates. Recrystallized grains, sub-grains, and deformed grains are indicated in blue, yellow, and red, respectively. At a strain rate of 10 s⁻¹ and varying defor-

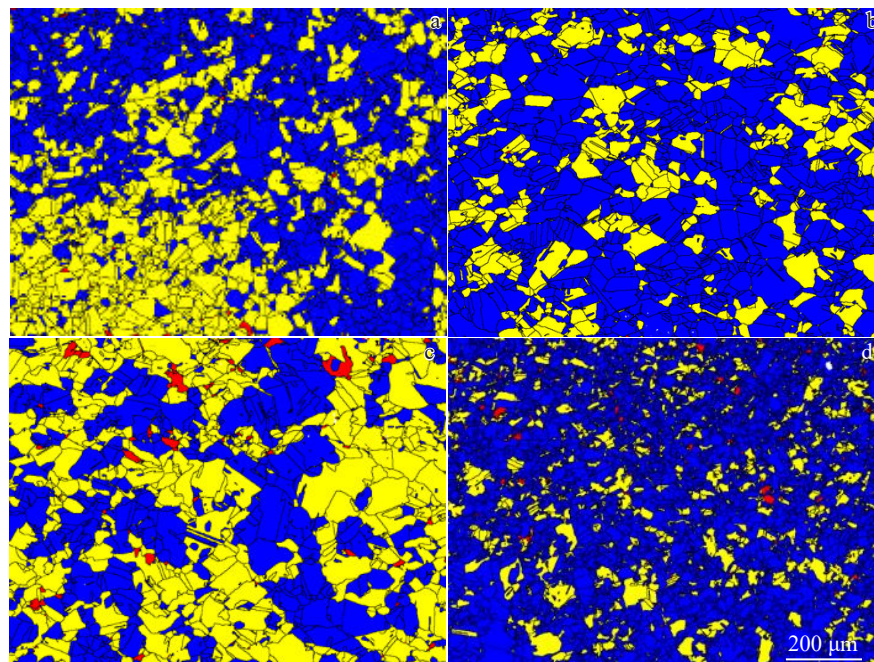


Fig.10 Distributions of dynamically recrystallized grains in electrolytic copper under different deformation conditions: (a) 600 °C, 10 s⁻¹; (b) 800 °C, 10 s⁻¹; (c) 500 °C, 0.01 s⁻¹; (d) 500 °C, 10 s⁻¹

mation temperatures (Fig. 10a–10b), the volume fraction of recrystallized grains notably increases to 58.3vol% and 71.7vol% at deformation temperatures of 600 and 800 °C, respectively. This phenomenon is attributed to the higher deformation temperature, which enhances atomic diffusion and accelerates grain boundary migration, resulting in a more complete recrystallization of electrolytic copper.

At low temperatures and low strain rates (Fig. 10c), the structure contains numerous sub-grains and a small number of deformed grains. The volume fraction of dynamically recrystallized grains in this scenario is 43.9vol%. This is because dynamic recrystallization, a thermally activated process during hot deformation, cannot fully complete at low temperatures and low strain rates.

Conversely, at low temperatures with high strain rates (Fig. 10d), dynamic recrystallization becomes more comprehensive with 80vol% recrystallized grains. The higher strain rates lead to significant strain energy accumulation within a brief deformation period, promoting recrystallization nucleation. However, the short duration impedes grain growth, leading to a considerable reduction in grain size despite the formation of numerous recrystallized grains.

4 Conclusions

1) Both the deformation temperature and strain rate exert a substantial influence on the thermal plastic deformation behavior of electrolytic copper. The flow stress gradually decreases with an increase in deformation temperature and a decrease in strain rate.

2) The calculated activation energy for deformation of electrolytic copper approximates 209.32 kJ/mol. The constitutive equation derived is:

$$\dot{\epsilon} = 8.11 \times 10^{10} [\sinh(0.01512\sigma)]^{6.29692} \exp\left(-\frac{209.32}{RT}\right)$$

3) Thermal processing maps reveal the optimal processing parameters for electrolytic copper at different strains, lying within deformation temperature range of 600–650 °C and strain rate range of 5–10 s⁻¹.

4) Under high-temperature plastic deformation condition, electrolytic copper primarily undergoes discontinuous dynamic recrystallization. As deformation temperature increases, grain coarsening is in close correlation with the extent of dynamic recrystallization. Conversely, at high strain rates (10 s⁻¹), there is a significant reduction in grain size.

References

- Xu Y T, Du H Y, Pei L et al. *Journal of Applied Electrochemistry*[J], 2023, 54: 597
- Li L, Shi Z M, Zhang L. *Rare Metal Materials and Engineering*[J], 2017, 46(12): 3589
- Zhang H M, Wang J, Liu G B et al. *International Journal of Material Forming*[J], 2020, 13: 479
- Song B X, Yu T B, Jiang X Y et al. *Journal of Materials Research and Technology*[J], 2020, 9(3): 6464
- Xu Yangtao, Pei Liang, Dai Jingmin et al. *Rare Metal Materials and Engineering*[J], 2023, 52(12): 4171 (in Chinese)
- Rezaei A H R, Shayanpoor A A. *Acta Metallurgica Sinica (English Letters)*[J], 2022, 35: 662
- Huang S H, Shu D Y, Hu C K et al. *Transactions of Nonferrous Metals Society of China*[J], 2016, 26(4): 1044
- Gronostajski Z. *Journal of Materials Processing Technology*[J], 2003, 142(3): 684
- Wang Xingmao, Ding Yutian, Gao Yubi et al. *Rare Metal Materials and Engineering*[J], 2022, 51(1): 249 (in Chinese)
- Zhang Y, Sun H L, Volinsky A A et al. *Journal of Materials Engineering and Performance*[J], 2016, 25: 1150
- Voisin T, Grapes M D, Li T T et al. *Materials Today*[J], 2020, 33: 10
- Huang S H, Chai S X, Xia X S et al. *Strength of Materials*[J], 2016, 48(1): 98
- Zolotarevsky N Y, Rybin V V, Matvienko A N et al. *Materials Characterization*[J], 2019, 147: 184
- Prasad Y, Rao K P. *Materials Science and Engineering A*[J], 2004, 374(1–2): 335
- Ji H C, Liu J P, Wang B Y et al. *Journal of Alloys and Compounds*[J], 2017, 693: 674
- Zhang Bing, Liu Pengru, Zhang Zhijuan et al. *Rare Metal Materials and Engineering*[J], 2022, 51(1): 203 (in Chinese)
- Sellars C M, McTegart W J. *Acta Metallurgica*[J], 1966, 14(9): 1136
- Sellars C M. *Metal Science*[J], 1979, 13(3–4): 187
- Jonas J J, Sellars C M, Tegart W J M G. *Metallurgical Reviews*[J], 1969, 14(1): 1
- Jenab A, Karimi Taheri A. *Materials Science and Technology*[J], 2011, 27(6): 1067
- Gao W, Belyakov A, Miura H et al. *Materials Science and Engineering A*[J], 1999, 265(1–2): 233
- Zener C, Hollomon J H. *Journal of Applied Physics*[J], 1944, 15(1): 22
- Shi Z X, Yan X F, Duan C H. *Journal of Alloys and Compounds* [J], 2015, 652: 30
- Rezaei A H R, Shayanpoor A A. *Physics of Metals and Metallography*[J], 2021, 122(13): 1426
- Cheng C, Tang Z Y, Zhao L et al. *Journal of Materials Engineering and Performance*[J], 2023, 32: 11432
- Ding W W, Chen S H, Hu L W et al. *Rare Metal Materials and Engineering*[J], 2023, 52(12): 4086

电解铜的热变形行为及微观组织演变

张 涵^{1,2}, 桑 晨^{1,2}, 张 燕³, 徐仰涛^{1,2}, 乔及森^{1,2}, 夏天东^{1,2}

(1. 兰州理工大学 材料科学与工程学院, 甘肃 兰州 730050)

(2. 兰州理工大学 省部共建有色金属先进加工与再利用国家重点实验室, 甘肃 兰州 730050)

(3. 金川集团铜业有限公司, 甘肃 金昌 737100)

摘 要: 在变形量70%的条件下, 通过Gleeble-3500热模拟试验机研究了电解铜在500~800 °C和0.01~10 s⁻¹范围内的热变形行为。分析电解铜在热变形过程中各变形参数下的真应力-真应变曲线, 建立了应变为0.5时的本构方程。在Prasad提出的动态材料模型基础上建立了不同应变下的加工图。同时, 采用电子背散射对压缩后的试样进行微观组织观察与分析。结果表明: 电解铜在高温塑性变形过程中对变形温度和应变速率表现出较强的敏感性, 随着温度的升高和应变速率的降低, 流变应力逐渐减小。根据加工图确定了电解铜的加工条件为变形温度600~650 °C, 应变速率5~10 s⁻¹。电解铜在高温塑性变形过程中发生了不连续动态再结晶, 在低温高应变速率下, 晶粒明显细化。

关键词: 电解铜; 热变形; 本构方程; 动态再结晶

作者简介: 张 涵, 女, 1978年生, 博士生, 兰州理工大学材料科学与工程学院, 甘肃 兰州 730050, E-mail: 18793138809@163.com